AGU ADVANCING EARTH AND SPACE SCIENCE

Geophysical Research Letters

RESEARCH LETTER
10.1029/2022GL099498

Key Points:

- A novel filter which includes vorticity and Doppler effects is used to extract near-inertial waves in a realistic ocean simulation
- Near-inertial energy is underestimated in anticyclonic flows and overestimated in cyclonic flows if both effects are omitted from the filter
- The anisotropic propagation of near-inertial waves in jets is only revealed when accounting for Doppler shifts in the wave filtering process

Correspondence to:
J. Rama,
jemima.rama@anu.edu.au

Citation:
Rama, J., Shakespeare, C. J., & Hogg, A. M. (2022). Importance of background vorticity effect and Doppler shift in defining near-inertial internal waves. *Geophysical Research Letters*, *49*, e2022GL099498. https://doi.org/10.1029/2022GL099498

Received 11 MAY 2022
Accepted 7 NOV 2022

Importance of Background Vorticity Effect and Doppler Shift in Defining Near-Inertial Internal Waves

Jemima Rama[1], Callum J. Shakespeare[1], and Andrew McC. Hogg[1]

[1]Research School of Earth Sciences, ARC Centre of Excellence in Climate Extremes, Australian National University, Canberra, ACT, Australia

Abstract Near-inertial waves contain a significant fraction of the ocean's internal wave energy and can propagate long distances from their source before dissipating. However, a varying background flow velocity can alter the wave propagation in two ways. The background vorticity modifies the lower bound of the wave frequency bandwidth while Doppler shifts alter the wave intrinsic frequency. Both effects complicate the identification of the waves and the quantification of their energy content. This study analyses the output of a realistic simulation of the North Pacific using adaptive frequency filters to isolate the effects of vorticity and Doppler shift on the apparent wave energy. Spectral filters neglecting background vorticity effects results in apparent near-inertial energy being underestimated by 40% in anticyclonic structures and overestimated by 100% in cyclonic structures. The asymmetry in energy bias is reinforced when both background vorticity and Doppler shift effects are omitted from the frequency filters.

Plain Language Summary In the ocean, motions that have an intrinsic frequency lower than the Coriolis frequency (f) are considered as slowly evolving flows such as vortices and currents, while motions with frequencies higher than f are oscillatory signals known as internal waves. Internal waves can propagate both horizontally and vertically through the ocean interior, thus allowing them to transmit energy and contribute to mixing in regions quite remote from their generation site. A subclass of internal waves are the near-inertial waves, generally identified as having frequencies just above f; however, turbulent background flows complicate the identification of such waves. For instance, ocean vortices modify the lower frequency cut-off of near-inertial internal waves while strong flows in jets shift the apparent wave frequency. This study shows that ignoring such modifications leads to a misidentification of near-inertial waves and to a poor capture of their propagation. As a result, the estimates of energy carried by near-inertial waves are significantly biased when the influence of vortices and jets is neglected from the filtering used to identify the waves.

1. Introduction

Near-inertial internal waves (NIWs) are typically defined as internal waves with frequencies slightly above the local inertial frequency f (Webster, 1968). The inertial frequency separates NIWs from geostrophic flows as well as from pure inertial motions, and thus ensures that internal waves can propagate into the ocean interior (Kroll, 1975). However, variations in background flow velocity and buoyancy can modulate the frequency cutoff above which NIWs exist and freely propagate (Mooers, 1975). In order to correctly identify NIWs, accurately capture their propagation and estimate their energy content without any bias, the frequency cutoff that separates non-wave motions from internal waves must be properly defined.

The background vertical vorticity modulates the lower bound of the frequency bandwidth over which internal waves exist. NIWs not only feel the Earth's rotation but also the fluid's relative rotation (Weller, 1982). NIWs experience the latitudinal variation in inertial frequency through β-refraction (D'Asaro et al., 1995) and the vertical relative vorticity through ζ-refraction (Balmforth & Young, 1999); both processes act to shrink the lateral scales of NIWs for more efficient propagation into the ocean interior (Thomas et al., 2020). ζ-refraction involves a shift of the inertial frequency (f) to the effective inertial frequency (f_{eff}) by background vertical relative vorticity (Mooers, 1975). The effective inertial frequency is defined as $f_{eff} = f + \overline{\zeta}/2$ for background relative vorticities characterized by $\zeta \leq 0.2f$ (Kunze, 1985), where $\overline{\zeta} = \frac{\partial \overline{v}}{\partial x} - \frac{\partial \overline{u}}{\partial y}$ and $\overline{u}$, $\overline{v}$ are the background horizontal velocities. Any shift of the frequency cutoff (from f to f_{eff}) separating the non-wave and wave components, significantly modifies the near-inertial energy (NIE) content given that the near-inertial peak and the bulk of wave energy are close to f. For instance, negative relative vorticity regions ($f_{eff} < f$) provide a broader frequency bandwidth

Geophysical Research Letters 10.1029/2022GL099498

for inertial resonance by the wind forcing (Whitt & Thomas, 2015) and for the generation of NIWs. Furthermore, NIWs generated in negative vorticity are likely to be trapped and fluxed downwards within anticyclonic structures (Asselin & Young, 2020; Danioux et al., 2008; Fu, 1981). In contrast, positive relative vorticity flows ($f_{eff} > f$) provide a narrower frequency bandwidth for inertial resonance and for the formation of NIWs. The waves triggered in cyclonic structures are inherently of higher frequency and are free to propagate away (Kunze & Sanford, 1984). A strong background vorticity field not only modifies the frequency bandwidth for inertial resonance but also displaces the turning point of NIWs, and thus re-organizes the spatial distribution of NIE (Klein et al., 2004). Consequently, neglecting the vorticity-induced shift of the frequency cutoff from f to f_{eff} when identifying NIWs may result in an incorrect interpretation of their dispersion and an erroneous estimation of their energy content, especially in eddy rich flows.

The background flow can alter the propagation of NIWs by modifying the intrinsic wave frequency, ω_i, which determines whether a NIW is freely propagating through, or evanescent in, a background flow. The intrinsic frequency in an unsteady, time-changing flow is defined as $\omega_i = \omega_o - \mathbf{k} \cdot \overline{\mathbf{u}}$ (Bühler, 2014), where ω_o is the observed Eulerian frequency, $\mathbf{k}$ is the horizontal wavenumber and $\overline{\mathbf{u}}$ is the horizontal background velocity. ω_i is the frequency intrinsic to local disturbance dynamics and is thus defined as the frequency "Doppler shifted" to an observer moving with the mean background flow relative to an observer who is at rest (Gill, 1982). The difference between ω_i and ω_o is in reality the "quasi-Doppler shift" (Gerkema et al., 2013), but is also commonly referred as the Doppler shift in past literature (Lighthill, 1978). In view of ray theory whereby ω_o (post wave generation) is conserved along a particular raypath in a steady flow, ω_i will adjust according to the Doppler shift $\left(\mathbf{k} \cdot \overline{\mathbf{u}}\right)$ (Bretherton & Garrett, 1968). The sign of the change in ω_i is then dependent on the propagation direction of the NIWs relative to the background flow velocity. If ω_i is lowered to f_{eff}, NIWs are more likely to hit a turning point and get deflected (Olbers, 1981). Conversely, if ω_i is shifted to higher frequencies, NIWs can propagate beyond their turning latitude (Zhai et al., 2004). Furthermore, in regions of strong Doppler shift, the intrinsic wave frequency (ω_i), and more importantly the corresponding Lagrangian near-inertial peak will differ from the observed frequency (ω_o) and associated Eulerian near-inertial peak. NIWs are typically defined as having intrinsic frequencies in the range $f < \omega_i < 1.2f$ (Alford et al., 2016), although a local bandwidth in terms of f_{eff} as described above would be more accurate. Large uncertainties are thus introduced in the identification of NIWs if the wave definition relies on ω_o, and if ω_o is different to ω_i. Defining NIWs based on their Eulerian frequency (ω_o) instead of their intrinsic frequency (ω_i) may introduce biases in the identification of NIWs and may hence inhibit the accurate description of their propagation, notably in strong background flows.

The relative magnitude of the effects of background vorticity and Doppler shift on NIWs depends on the scale of the waves, and more importantly, on the angle of incidence of the waves when impinging a geostrophic current. To illustrate the interplay of both effects, we consider NIWs propagating toward a strong geostrophic current, such as the extension of the Kuroshio. When waves propagate perpendicularly to the flow direction, the Doppler shift $\left(\mathbf{k} \cdot \overline{\mathbf{u}}\right)$ is zero and the effects of background vorticity are likely to dominate. Conversely, when NIWs impinge the front at a smaller angle, almost along-front, the Doppler shift is more likely to overcome vorticity effects (Kunze, 1985), especially for small-scale (high $\mathbf{k}$) NIWs which experience the effects of the Doppler shift more strongly than their large-scale counterparts (Pinkel, 2008). The interplay of the background vorticity and Doppler shift on the definition of NIWs is thus a strong function of the direction of wave propagation relative to the background flow and wavelength.

Past idealized studies have examined the effects of vorticity and Doppler shift on NIWs propagation through ray tracing (Kunze, 1985; Whitt & Thomas, 2013), while observational studies (Alford et al., 2013; Cuypers et al., 2013; Lelong et al., 2020) have corroborated theoretical predictions of the modifications in wave propagation due to the vorticity shift of f and the Doppler shift of ω_i. Nevertheless, the subtleties in the variations of the frequency cutoff (f_{eff}) and in the Doppler shift of ω_i are rarely considered when NIWs are extracted from the output of realistic simulations (Furuichi et al., 2008; Joyce et al., 2013; Lee & Niiler, 1998). NIWs are typically filtered based on their Eulerian frequency (Zhai et al., 2007, 2009), and the filter cutoff is set to the inertial frequency (f). Energy exchanges between geostrophic flows and NIWs are also generally evaluated with respect to f rather than f_{eff} (Barkan et al., 2021; Jing et al., 2017). In this study, we aim to correctly identify NIWs by including the effects of vorticity and Doppler shift in the extraction of NIWs from a realistic model simulation of wind-generated NIWs near the extension of the Kuroshio. The basis of our method relies on comparing the use of f and f_{eff} as frequency cutoffs to extract the NIW component. The difference in NIE, estimated from filtered wave fields using f versus f_{eff}, highlights the fraction of NIE associated with the background vorticity effects. In

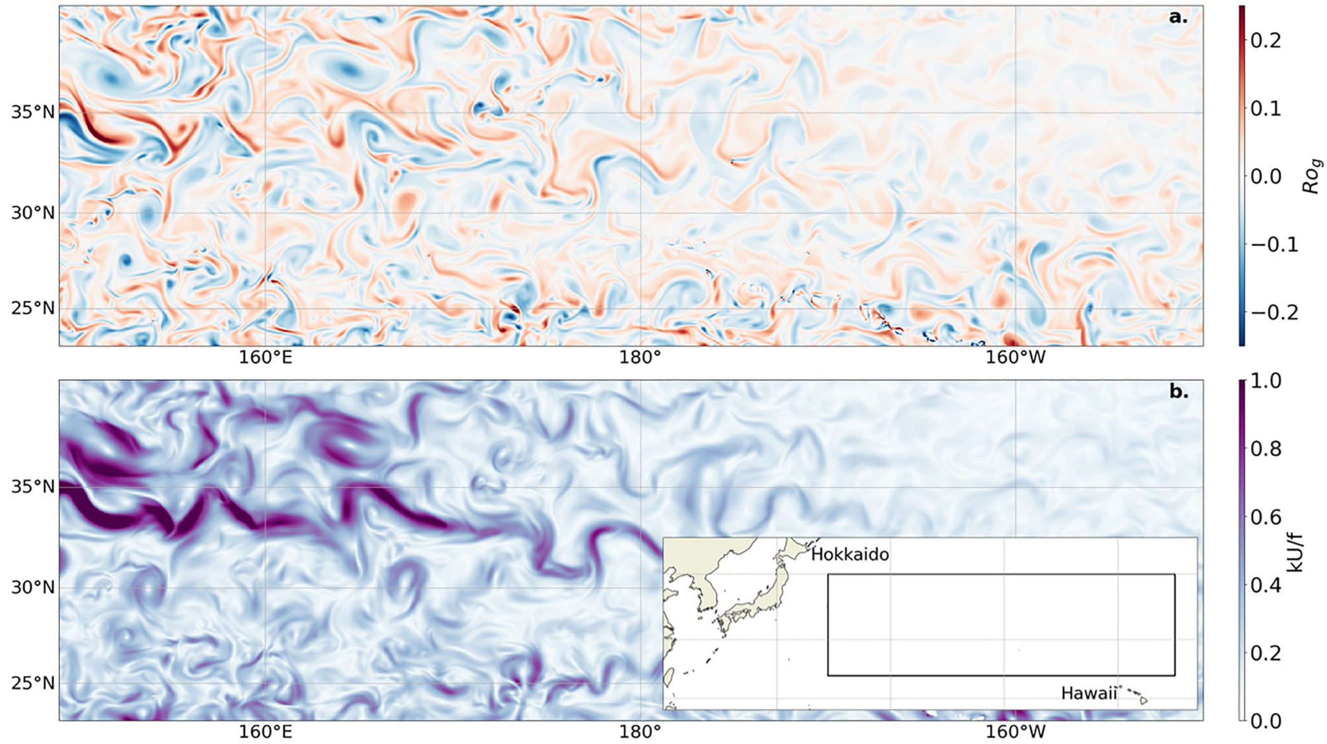

Figure 1. (a) Rossby number ($Ro_g = (f_{eff} - f)/f$) and (b) the upper bound for the Doppler shift (kU/f), where k is set to 1/10 km (10 km is the smallest horizontal wavelength resolved by the model) and U is the speed of the background flow at 100 m depth. Values of f_{eff} and U have been averaged over 3 days. The inset in (b) shows the location (black box) of the study region.

addition, our methodology compares the application of the spectral filter in both the Eulerian and the Lagrangian frame. As opposed to filtering NIWs on a Eulerian frame, extracting NIWs in a Lagrangian filtering uncovers any trapped waves that are otherwise buried in the sub-inertial component. We demonstrate that incorporating both the effects of background vorticity and Doppler shift in the extraction of NIWs is essential for adequately resolving the propagation of the waves and estimating their energy content.

2. Methods

MITgcm (Marshall et al., 1997) is used to simulate a sub-section of the western North Pacific Ocean, described in Rama et al. (2022). The horizontal grid spacing of the model is 5 km while the vertical grid consists of 200 vertical levels. The selected region provides an ideal domain for the study of the propagation of near-inertial waves in a rich mesoscale field as shown in Figure 1. The existing turbulent eddy field provides a wide range of background vorticities (Figure 1a) for trapping and expulsion of NIWs while the extension of the Kuroshio current creates a strong front (Figure 1b) where the waves can experience the Doppler shift effects. The Rossby number is defined as $Ro_g = (f_{eff} - f)/f$ and the extent of the Doppler shift effect is estimated as kU/f, where k is the horizontal wavenumber for the smallest NIWs resolved in the model ($k = 1/10$ km) and U is the speed of the background flow. There is no tidal forcing in the simulation. Our study analyses NIWs triggered in the wake of a storm system that traversed north of the extension of the Kuroshio from 4 to 7 April 2006. All following analyses are thus restricted to the model output from 6 to 13 April 2006, directly following the storm event.

We employ four different high-pass frequency filters to extract the wave component from the model output; each frequency filter incorporates the effects of background vorticity, Doppler shift, neither, or both effects into the identification of NIWs. The frequency filters are defined as follows: (a) $Eulerian_f$ and (b) $Eulerian_{feff}$ which are filters in the Eulerian frame and (c) $Lagrangian_f$ and (d) $Lagrangian_{feff}$ which are filters in the Lagrangian frame. The subscripts represent the respective filter cutoffs at f and f_{eff}. We argue that the $Lagrangian_{feff}$ filter correctly identifies NIWs since it incorporates variations in background vorticity in the frequency cutoff and extracts waves based on the intrinsic frequency spectrum (ω_i). Near-inertial energy (NIE) computed from filtered wave fields of

$Lagrangian_{feff}$ is considered to be closest to the "true" value of NIE present in the simulation. The wave energy computed from the other filters is only the "apparent" wave energy when either, or both, vorticity and Doppler shift effects are ignored when extracting NIWs. Our analysis compares the "apparent" with the "true" NIE in order to calculate the fraction of wave energy that is either underestimated or overestimated when background vorticity and Doppler shift effects are neglected from the wave filter.

All 4 types of filtering employed in this study rely on the Lagrangian filtering package described in Shakespeare et al. (2021), which has been extended to support adaptive frequency cutoffs in the Butterworth high-pass frequency filter. While f has a latitudinal dependence, f_{eff} depends on the background vorticity which varies over space and through time. We compute f_{eff} from hourly velocity fields that have been averaged over 29 hr. In addition, the 4 filters employ a total time window of 6 days for frequency filtering. In the Lagrangian frame, the particles are advected 3 days backwards and 3 days forward in time prior to spectral filtering. A time series of 6 days keeps the Lagrangian particles within the same relative vorticity regime during advection, and also ensures a frequency resolution that can differentiate between f and f_{eff} in Fourier space. The four frequency filters are applied to the model output and each set of filtered wave fields, u' and v' (where u' and v' are the wave contributions to the zonal and meridional velocity, respectively), is used to estimate the NIW kinetic energy (KE). Under the assumption that NIWs have small vertical wavelengths and that their available potential energy is much smaller than their KE (Alford et al., 2016), the wave KE is considered to be a good proxy for the overall NIE. The following analyses examine the internal wave KE, which is hereafter also defined as NIE since the bulk of the wave energy lies in the near-inertial band. We estimate 4 sets of KE, each of which has been computed from filtered wave fields of $Eulerian_f$, $Eulerian_{feff}$, $Lagrangian_f$ and $Lagrangian_{feff}$, respectively.

A comparison between individual estimates of KE allows us to isolate the bias in NIE when either the background vorticity, or Doppler shift, or both effects are omitted from the extraction of the NIW component. The biases in NIE are defined as percentage differences: $[(Apparent\ energy - True\ energy)/True\ energy] \times 100$. We first define the term ζ_{bias} as the percentage difference between estimates of apparent KE from $Lagrangian_f$ and "true" KE from $Lagrangian_{feff}$. ζ_{bias} highlights the percentage of "true" NIE that is either underestimated or overestimated when vorticity shifts in the frequency cutoff are neglected. We introduce a second term, σ_{bias} as the percentage difference between estimates of apparent KE from $Eulerian_{feff}$ and "true" KE from $Lagrangian_{feff}$. σ_{bias} displays the fraction of "true" NIE which is either underestimated or overestimated when Doppler shift effects are excluded from the wave filtering process. For instance, extracting NIWs in a Eulerian frame may result in sub-inertial waves being erroneously identified as non-wave flows, or inversely, sub-mesoscale motions being classified as part of the wave component. Finally, the term $\zeta\sigma_{bias}$ exposes the bias in NIE when both effects of background vorticity and Doppler shift are omitted from the extraction of NIWs. $\zeta\sigma_{bias}$ is computed as the percentage difference between apparent KE from $Eulerian_f$ and "true" KE from $Lagrangian_{feff}$. We note that the bias associated with employing different filter shapes, such as different orders of the Butterworth filter, is negligible in comparison to the bias introduced when using the four types of filter. The following sections examine the terms ζ_{bias}, σ_{bias} and $\zeta\sigma_{bias}$, and highlight the bias in estimated NIE when effects of background vorticity and Doppler shifts are ignored from the definition of NIWs.

3. Results

3.1. Bias in Apparent Near-Inertial Energy

Figure 2 shows the distribution of the bias in apparent NIE when neglecting effects of vorticity (ζ_{bias}), Doppler shift (σ_{bias}) and a combination of both effects ($\zeta\sigma_{bias}$) from the identification of NIWs. The KE from respective filtered fields is computed separately at every time step and averaged over 3 days prior to computing ζ_{bias}, σ_{bias}, and $\zeta\sigma_{bias}$.

The imprint of the mesoscale structures is reflected in the distribution of ζ_{bias} (Figure 2a), whereby the apparent NIE is underestimated in anticyclonic flows ($\zeta_{bias} < 0$) and overestimated in cyclonic structures ($\zeta_{bias} > 0$). ζ_{bias} is asymmetric across the background vorticity range; the apparent wave energy is underestimated by 30% at $Ro_g = -0.05$ and overestimated by 40% at $Ro_g = 0.05$ when vorticity effects are not factored into the wave extraction process. Figure 2a also demonstrates that excess NIE in anticyclonic eddies and wave energy deficit in cyclonic vortices are not adequately resolved when filtering NIWs using the $Lagrangian_f$ filter. Based on the "true" wave energy estimated from filtered fields of $Lagrangian_{feff}$ (figure not shown), strong anticyclonic regions

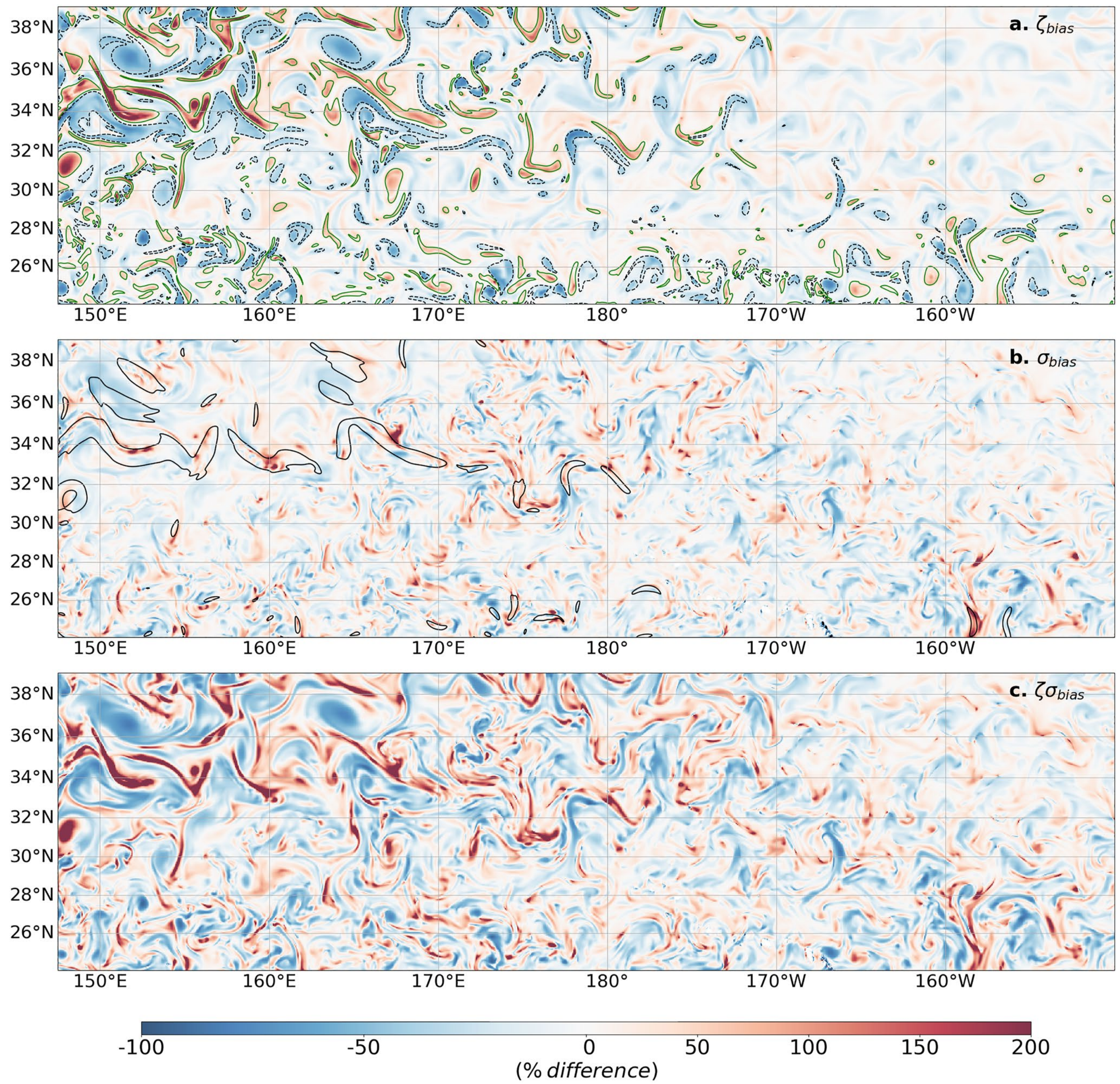

Figure 2. Percentage error in calculated NIW energy when (a) vorticity, (b) Doppler shift, and (c) both effects are neglected from the wave filtering. The ratios are computed from NIW KE at 100 m, that have been averaged over 3 days (7–10 April 2006). Dashed black contours enclose regions of $Ro_g < -0.05$ and green contours enclose areas of $Ro_g > 0.05$ in (a) Black contours enclose regions of $kU/f > 0.6$ in (b).

trap more wave energy; areas of $Ro_g = -0.2$ experience 20% more near-inertial energy on average than regions characterized by $Ro_g = -0.1$. Conversely, for cyclonic flows, the wave energy present in regions of $Ro_g = 0.2$ is half the energy in areas of $Ro_g = 0.1$. The redistribution of NIE by background vorticity is hence poorly captured when NIWs are extracted based on a cutoff of f instead of f_{eff}.

Figure 2b shows the spatial distribution in σ_{bias}. The absence of a distinct distribution in σ_{bias} is expected given that our methodology does not separate the biases associated with the individual influences of a positive versus negative Doppler shift. σ_{bias} hence showcases the error in the estimated apparent wave energy when combined effects of positive and negative Doppler shifts are ignored from the wave filtering. Nevertheless, the distribution of σ_{bias} can give an insight into the dominant propagating direction of NIWs as they impinge strong fronts. For example,

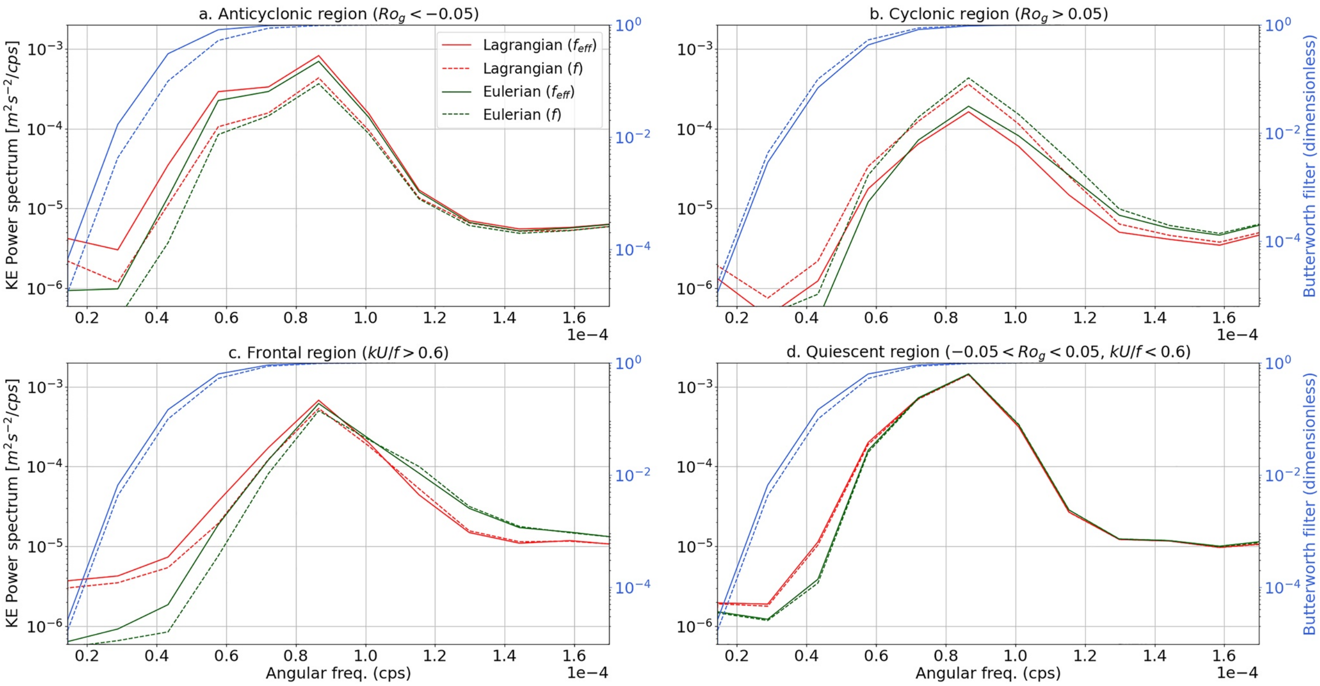

Figure 3. KE spectra computed from the four sets of filtered wave fields. All four spectra shown for (a) Anticyclonic flows, (b) Cyclonic flows, (c) Frontal flows, and (d) Quiescent regions at 100 m depth. The dimensionless fourth order Butterworth filters are shown in blue and plotted on the secondary *y*-axis. f (dash line) and f_{eff} (solid line) at the lowest latitude in each region is represented. The minimum f_{eff} is shown for anticyclonic flows (a) and the maximum f_{eff} is shown for cyclonic flows (b). Both the minimum and maximum f_{eff} are shown in (c and d).

the wave energy is overestimated ($\sigma_{bias} > 0$) on the cyclonic edge of the Kuroshio extension, which suggests that NIWs are propagating predominantly against the background flow ($\omega_i > \omega_o$). In this regard, an Eulerian filter might misidentify balanced motions as NIWs, hence contributing to an overestimation of the apparent NIE. In contrast, when NIWs disperse along front with the background flow ($\omega_i < \omega_o$), the Eulerian filter classifies NIWs as part of the balanced flow and the apparent NIE is underestimated ($\sigma_{bias} < 0$). σ_{bias} reveals the percentage of NIE which is underestimated when the NIWs disperse mainly with the background front or overestimated when the waves are more likely propagating against the background flow.

Lastly, Figure 2c shows the distribution in $\zeta\sigma_{bias}$, whereby the asymmetry in the bias across the vorticity range is reinforced. The apparent wave energy is underestimated by 35% at $Ro_g = -0.05$ and overestimated by 55% at $Ro_g = 0.05$, with $\zeta\sigma_{bias}$ reaching an overestimation of 200% in very strong cyclonic frontal structures. The amplified asymmetry in $\zeta\sigma_{bias}$ thus shows that excluding both background vorticity and Doppler shift effects from the identification of NIWs results in an overall underestimation of NIE in anticyclonic flows and overestimation of energy in cyclonic structures.

3.2. Changes in Near-Inertial Wave Frequency Spectrum

The influence of the background vorticity and Doppler shifts is reflected on the shape of the NIE frequency spectra. Figure 3 shows the KE spectra associated with the 4 adaptive frequency filters, averaged over different flow regimes. Each frequency spectrum is computed from a time series of filtered velocity fields of 5 days, whereby the respective time series are tapered using a Kaiser window ($\alpha = 3$) prior to applying the Fourier transform. The flow regimes selected include anticyclonic structures ($Ro_g < -0.05$), cyclonic structures ($Ro_g > 0.05$), strong frontal jets ($kU/f > 0.6$) and quiescent flows ($-0.05 < Ro_g < 0.05$, $kU/f < 0.6$). We highlight that we are not comparing spectra between these regions since conditions such as the wind-forcing and stratification vary across the domain. Instead, we compare the spectra from the four adaptive filters within the individual flow regimes. In anticyclonic regions (Figure 3a), the near-inertial peak bandwidth is broadened and the peak height is almost doubled from $4 \times 10^{-4} m^2s^{-2}$ (filter based on f) to $8 \times 10^{-4} m^2s^{-2}$ (filter based on f_{eff}). Conversely, in cyclonic regions (Figure 3b), the near-inertial peak is lowered from $3.5 \times 10^{-4} m^2s^{-2}$ (filter based on f) to $1.6 \times 10^{-4} m^2s^{-2}$

10.1029/2022GL099498

(filter based on f_{eff}) and shows a narrower bandwidth. The modifications in the shape of the near-inertial peak results from the adaptive frequency cutoff, which is allowed to shift with variations in the background vorticity. In frontal regions (Figure 3c), the Lagrangian-filtered spectrum is shifted to lower frequencies with respect to the Eulerian-filtered spectrum. The background flows defined as $kU/f > 0.6$ are predominantly in negative vorticity regions, and reduced values of f_{eff} contribute to the shift of the Lagrangian-filtered spectrum toward lower frequencies. On the other hand, the quiescent region (Figure 3d) serves as a control and shows that the four spectra are relatively similar. Without variations in background vorticity, the frequency cutoff f_{eff} approaches f, while the absence of a strong frontal flow implies that NIWs are not significantly shifted to lower or higher frequencies. We note that the flattening of the spectral slope at the lowest frequencies ($\omega < 0.4 \times 10^{-4}$) in Figure 3 is an artifact created by the concatenation of filtered wave fields over time. The KE spectra, and hence the NIE content, are primarily modified in eddy-rich fields and in strong frontal jets; such dynamic conditions are usually present in the vicinity of western boundary currents.

3.3. Combined Effects of Background Vorticity and Doppler Shift

The terms ζ_{bias}, σ_{bias} and $\zeta\sigma_{bias}$ are regrouped and classified by values of background vorticity and Doppler shift in (Figure 4). ζ_{bias}, σ_{bias} and $\zeta\sigma_{bias}$ are computed over the whole horizontal domain and at selected depths from the surface to 2,000 m. Each term is associated with prevailing values of background vorticity (Ro_g) and Doppler shift (kU/f), which are subsequently employed to bin ζ_{bias}, σ_{bias} and $\zeta\sigma_{bias}$. As such, the values shown in Figure 4 represent the domain-mean NIE bias for a given flow speed and vorticity. In view of ζ_{bias} (Figure 4a), an asymmetry is observed across the background vorticity range; the apparent NIE is underestimated by 35% at $Ro_g = -0.1$ and is overestimated by 100% at $Ro_g = 0.1$. With regards to σ_{bias} (Figure 4b), the apparent wave energy is generally overestimated across a wide range of Doppler shifts. Moreover, $\sigma_{bias} > 0$ suggests an asymmetry in $\mathbf{k} \cdot \mathbf{u}$ whereby a higher fraction of NIWs are propagating against the background flow compared to NIWs propagating in the same direction as background flow. Finally, the interplay of neglecting both background vorticity and Doppler shift when estimating the NIE is highlighted by $\zeta\sigma_{bias}$ in Figure 4c. The asymmetry in the apparent energy bias is further reinforced; the underestimation of NIE is slightly greater (40% at $Ro_g < -0.1$) in anticyclonic flows and wave energy overestimation is further amplified in cyclonic flows (150% at $Ro_g > 0.1$). Thus, in regions of strong background flows and turbulent eddy fields, such as near western boundary currents where Ro_g is typically 0.1 or larger, the magnitude of the bias in apparent wave energy is at least 40% when vorticity and Doppler shift effects are not included in the filtering of NIWs.

3.4. Anisotropic Propagation of Near-Inertial Waves

Taking into account the background vorticity and Doppler shift effects when defining NIWs reveals a preferential propagation for NIWs, whereby the waves propagate against strong background flows. Figure 5 shows that the near-inertial horizontal energy flux is contingent upon the definition of NIWs. The uni-directional propagation of NIWs is not resolved when vorticity effects, and more importantly, when Doppler shifts are neglected from the filtering of NIWs. The wave horizontal energy flux (shown by quivers in Figure 5) is computed as $\mathbf{u}'p'$, where $\mathbf{u}'$ is the wave horizontal velocity vector and p', the wave pressure perturbation (Nash et al., 2005). We define three sets of apparent horizontal energy fluxes which lack the effects of both vorticity and Doppler shifts (Figure 5a), only vorticity (Figure 5b) and only Doppler shift (Figure 5c) in the NIWs definition. The horizontal flux closest to the "true" horizontal flux is computed from the filtered wave fields of $Lagrangian_{feff}$ (Figure 5d). When vorticity effects are resolved in the filters (Figures 5b and 5d), the wave horizontal energy flux into anticyclonic eddies (black boxes in Figure 5) is ≈60% higher, suggesting that "inertial trapping" (Lee & Niiler, 1998) is better represented. In addition, incorporating Doppler shift effects into the definition of the waves (Figures 5c and 5d) reveals the net anisotropic propagation of NIWs (blue boxes in Figure 5), with the wave horizontal energy flux being ≈200% higher on the cyclonic side of the extension of the Kuroshio. The preferential propagation of the waves can be explained by the modifications in the intrinsic wave frequency. NIWs approaching the front in the same direction as the background flow will tend to become more inertial (ω_i decreases) and will ultimately hit their turning point before getting deflected away. Conversely, if NIWs impinge the front while propagating against the background flow, the waves will get less inertial (ω_i increases) and will be able to propagate further into the jet. Strong background flows can therefore act as valves (Olbers, 1981) and selectively trap NIWs propagating against the flow (Kunze, 1985). A comparison between Figure 5d and Figure 5a suggests that background vorticity and

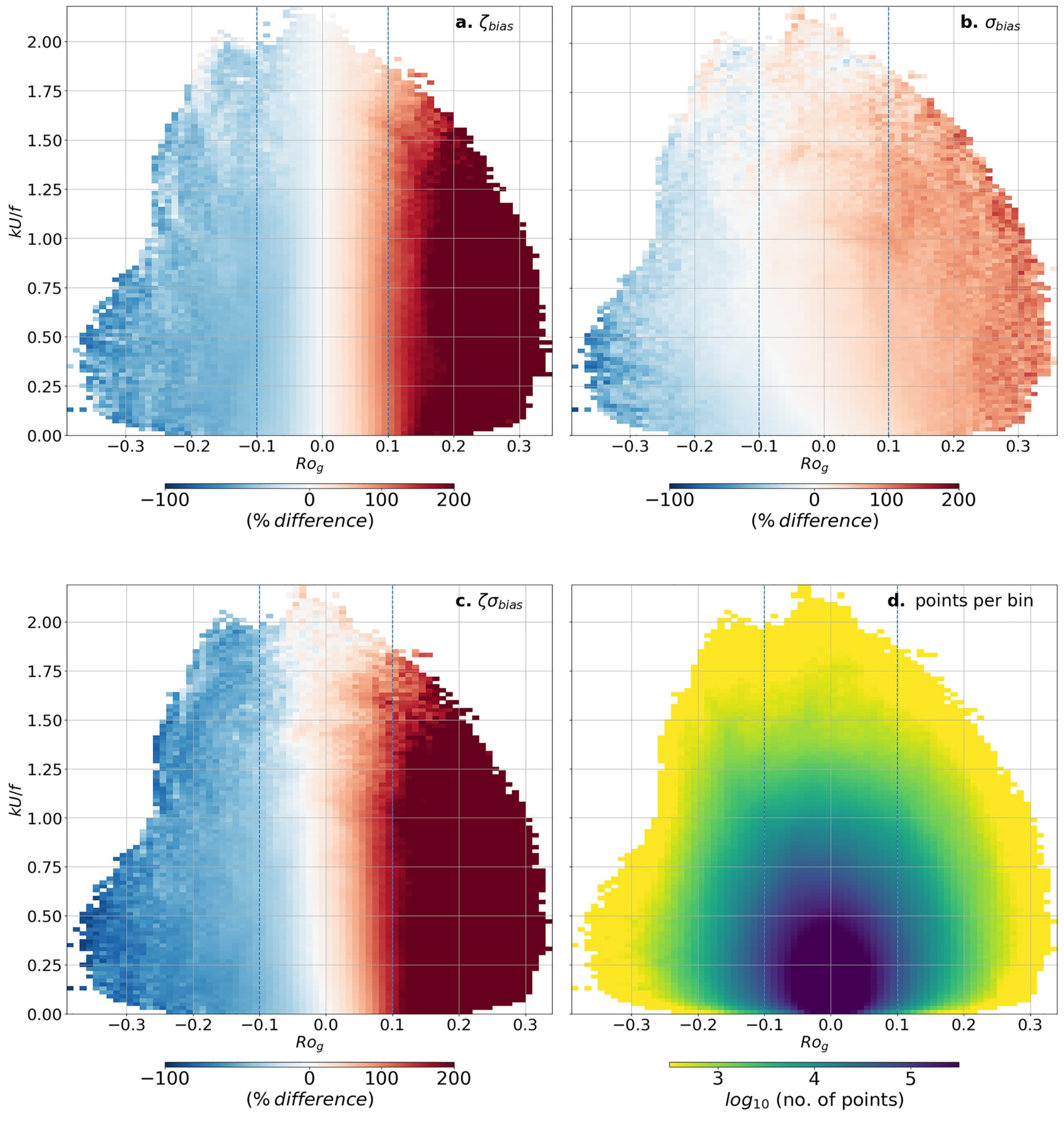

Figure 4. (a) ζ_{bias}, (b) σ_{bias}, and (c) $\zeta\sigma_{bias}$ regrouped and binned as per values of Ro_g and kU/f. All terms have been previously computed over the whole domain and at selected depths from the surface to 2,000 m. Data is taken from 7 to 12 April 2006. Number of points in each bin is shown in (d) Bins which contain less than 100 data points are excluded from the plots.

Doppler shifts act in concert to redirect NIWs propagation, promoting dispersion of waves propagating against the direction of background flows. Therefore, the preferential propagation of NIWs in the vicinity of strong fronts can only be observed if the background vorticity effects and Doppler shift are considered when extracting the NIW signal.

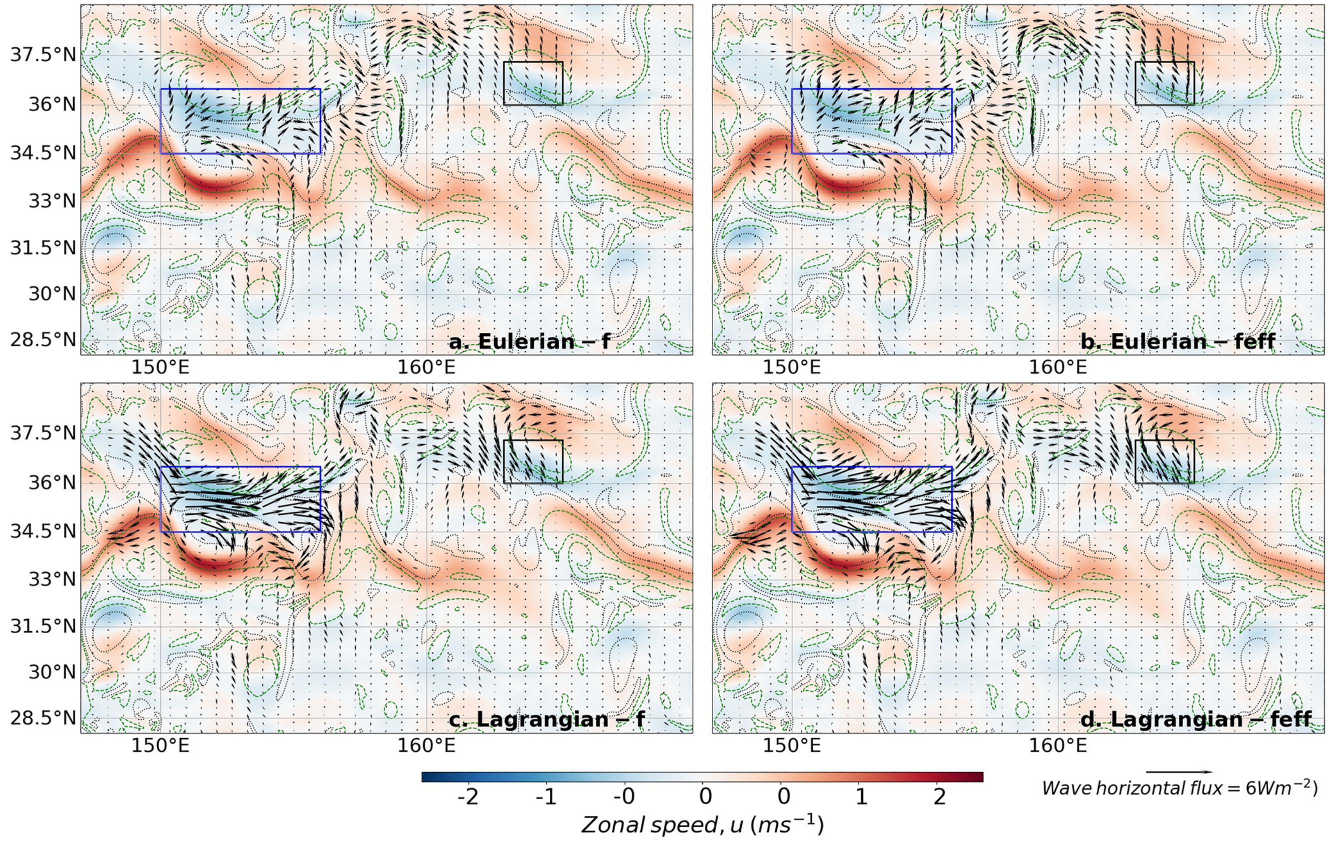

Figure 5. Horizontal flux of NIWs when the definition of the waves includes (a) neither vorticity effects nor Doppler shift (b) only vorticity effects (c) only Doppler shift and (d) both vorticity effects and Doppler shift. Quivers show the horizontal flux of the NIWs, integrated over a period of 3 days, and the contours represent the mean zonal speed (U) at 100 m. Dashed black contours enclose regions of $Ro_g > 0.05$ and green contours enclose areas of $Ro_g < -0.05$. The boxes highlight regions of interest.

4. Conclusion

This study estimates the bias in apparent near-inertial energy (NIE) when background vorticity and Doppler shift effects are ignored when defining NIWs. The exclusion of both effects results in an asymmetric bias whereby the apparent wave energy is underestimated in anticyclonic flows (by 40% at $Ro_g = -0.1$) and overestimated in cyclonic structures (by 100% at $Ro_g = 0.1$). The redistribution of NIE by background vorticity is only partially captured when NIW filtering relies on f instead of f_{eff}. Furthermore, wave filters that neglect Doppler shift effects fail to resolve the preferential propagation of NIWs. Omitting both background vorticity and Doppler shift in the definition of NIWs leads to an erroneous description of the wave propagation and a biased estimate of the NIE content. The inclusion of background vorticity and Doppler shift effects is therefore warranted when extracting the NIW component of the flow for the correct estimation of the wave energy and fluxes.

Acknowledgments

The authors would like to thank Angus Gibson for the development of the "Lagrangian Filtering" library and for his guidance on the usage of the package. We are also grateful to Ross Griffiths and two anonymous reviewers for their helpful suggestions on the manuscript. JR acknowledges support from the Australian Government's Research Training Program (AGRTP). CJS acknowledges support from an Australian National University Futures Scheme award. Numerical simulations and analyses were conducted on the National Computational Infrastructure (NCI) facility, Canberra, Australia.

Data Availability Statement

This work is based on output from high-resolution numerical models; model configuration files can be accessed on https://doi.org/10.5281/zenodo.6540699 and the Lagrangian filtering library can be accessed on https://lagrangian-filtering.readthedocs.io/.

References

Alford, M. H., MacKinnon, J. A., Simmons, H. L., & Nash, J. D. (2016). Near-inertial internal gravity waves in the ocean. *Annual Review of Marine Science*, *8*(1), 95–123. https://doi.org/10.1146/annurev-marine-010814-015746

Alford, M. H., Shcherbina, A. Y., & Gregg, M. C. (2013). Observations of near-inertial internal gravity waves radiating from a frontal jet. *Journal of Physical Oceanography*, *43*(6), 1225–1239. https://doi.org/10.1175/jpo-d-12-0146.1

Asselin, O., & Young, W. R. (2020). Penetration of wind-generated near-inertial waves into a turbulent ocean. *Journal of Physical Oceanography*, *50*(6), 1699–1716. https://doi.org/10.1175/jpo-d-19-0319.1

Balmforth, N. J., & Young, W. R. (1999). Radiative damping of near-inertial oscillations in the mixed layer. *Journal of Marine Research*, *57*(4), 561–584. https://doi.org/10.1357/002224099321549594

Barkan, R., Srinivasan, K., Yang, L., McWilliams, J. C., Gula, J., & Vic, C. (2021). Oceanic mesoscale eddy depletion catalyzed by internal waves. *Geophysical Research Letters*, *48*(18), e2021GL094376. https://doi.org/10.1029/2021gl094376

Bretherton, F. P., & Garrett, C. J. R. (1968). Wavetrains in inhomogeneous moving media. *Proceedings of the Royal Society of London. Series A. Mathematical and Physical Sciences*, *302*(1471), 529–554.

Bühler, O. (2014). *Waves and mean flows*. Cambridge University Press.

Cuypers, Y., Le Vaillant, X., Bouruet-Aubertot, P., Vialard, J., & Mcphaden, M. J. (2013). Tropical storm-induced near-inertial internal waves during the Cirene experiment: Energy fluxes and impact on vertical mixing. *Journal of Geophysical Research: Oceans*, *118*(1), 358–380. https://doi.org/10.1029/2012jc007881

Danioux, E., Klein, P., & Rivière, P. (2008). Propagation of wind energy into the deep ocean through a fully turbulent mesoscale eddy field. *Journal of Physical Oceanography*, *38*(10), 2224–2241. https://doi.org/10.1175/2008jpo3821.1

D'Asaro, E. A., Eriksen, C. C., Levine, M. D., Niiler, P., & Van Meurs, P. (1995). Upper-ocean inertial currents forced by a strong storm. Part I: Data and comparisons with linear theory. *Journal of Physical Oceanography*, *25*(11), 2909–2936. https://doi.org/10.1175/1520-0485(1995)025<2909:uoicfb>2.0.co;2

Fu, L.-L. (1981). Observations and models of inertial waves in the deep ocean. *Reviews of Geophysics*, *19*(1), 141–170.

Furuichi, N., Hibiya, T., & Niwa, Y. (2008). Model-predicted distribution of wind-induced internal wave energy in the world's oceans. *Journal of Geophysical Research*, *113*(C9), C09034. https://doi.org/10.1029/2008jc004768

Gerkema, T., Maas, L. R., & van Haren, H. (2013). A note on the role of mean flows in Doppler-shifted frequencies. *Journal of Physical Oceanography*, *43*(2), 432–441. https://doi.org/10.1175/jpo-d-12-090.1

Gill, A. E. (1982). *Atmosphere-ocean dynamics* (Vol. 30). Academic Press.

Jing, Z., Wu, L., & Ma, X. (2017). Energy exchange between the mesoscale oceanic eddies and wind-forced near-inertial oscillations. *Journal of Physical Oceanography*, *47*(3), 721–733. https://doi.org/10.1175/jpo-d-16-0214.1

Joyce, T. M., Toole, J. M., Klein, P., & Thomas, L. N. (2013). A near-inertial mode observed within a Gulf Stream warm-core ring. *Journal of Geophysical Research: Oceans*, *118*(4), 1797–1806. https://doi.org/10.1002/jgrc.20141

Klein, P., Smith, S. L., & Lapeyre, G. (2004). Organization of near-inertial energy by an eddy field. *Quarterly Journal of the Royal Meteorological Society*, *130*(598), 1153–1166. https://doi.org/10.1256/qj.02.231

Kroll, J. (1975). The propagation of wind-generated inertial oscillations from the surface into the deep ocean. *Journal of Marine Research*, *33*, 15–51.

Kunze, E. (1985). Near-inertial wave propagation in geostrophic shear. *Journal of Physical Oceanography*, *15*(5), 544–565. https://doi.org/10.1175/1520-0485(1985)015<0544:niwpig>2.0.co;2

Kunze, E., & Sanford, T. B. (1984). Observations of near-inertial waves in a front. *Journal of Physical Oceanography*, *14*(3), 566–581. https://doi.org/10.1175/1520-0485(1984)014<0566:ooniwi>2.0.co;2

Lee, N., & Niiler, P. P. (1998). The inertial chimney: The near-inertial energy drainage from the ocean surface to the deep layer. *Journal of Geophysical Research*, *103*(C4), 7579–7591. https://doi.org/10.1029/97jc03200

Lelong, M.-P., Cuypers, Y., & Bouruet-Aubertot, P. (2020). Near-inertial energy propagation inside a Mediterranean anticyclonic eddy. *Journal of Physical Oceanography*, *50*(8), 2271–2288. https://doi.org/10.1175/jpo-d-19-0211.1

Lighthill, J. (1978). *Waves in fluids*. Cambridge University Press.

Marshall, J., Adcroft, A., Hill, C., Perelman, L., & Heisey, C. (1997). A finite-volume, incompressible Navier Stokes model for studies of the ocean on parallel computers. *Journal of Geophysical Research*, *102*(C3), 5753–5766. https://doi.org/10.1029/96jc02775

Mooers, C. N. (1975). Several effects of a baroclinic current on the cross-stream propagation of inertial-internal waves. *Geophysical & Astrophysical Fluid Dynamics*, *6*(3), 245–275. https://doi.org/10.1080/03091927509365797

Nash, J. D., Alford, M. H., & Kunze, E. (2005). Estimating internal wave energy fluxes in the ocean. *Journal of Atmospheric and Oceanic Technology*, *22*(10), 1551–1570. https://doi.org/10.1175/jtech1784.1

Olbers, D. J. (1981). The propagation of internal waves in a geostrophic current. *Journal of Physical Oceanography*, *11*(9), 1224–1233. https://doi.org/10.1175/1520-0485(1981)011<1224:tpoiwi>2.0.co;2

Pinkel, R. (2008). Advection, phase distortion, and the frequency spectrum of finescale fields in the sea. *Journal of Physical Oceanography*, *38*(2), 291–313. https://doi.org/10.1175/2007jpo3559.1

Rama, J., Shakespeare, C. J., & Hogg, A. M. (2022). The wavelength dependence of the propagation of near-inertial internal waves. *Journal of Physical Oceanography*, *52*(10), 2493–2514. https://doi.org/10.1175/jpo-d-21-0266.1

Shakespeare, C. J., Gibson, A. H., Hogg, A. M., Bachman, S. D., Keating, S. R., & Velzeboer, N. (2021). A new open source implementation of Lagrangian filtering: A method to identify internal waves in high-resolution simulations. *Journal of Advances in Modeling Earth Systems*, *13*(10), e2021MS002616. https://doi.org/10.1029/2021ms002616

Thomas, L. N., Rainville, L., Asselin, O., Young, W. R., Girton, J., Whalen, C. B., et al. (2020). Direct observations of near-inertial wave ζ-refraction in a dipole vortex. *Geophysical Research Letters*, *47*(21), e2020GL090375. https://doi.org/10.1029/2020gl090375

Webster, F. (1968). Observations of inertial-period motions in the deep sea. *Reviews of Geophysics*, *6*(4), 473–490. https://doi.org/10.1029/rg006i004p00473

Weller, R. A. (1982). The relation of near-inertial motions observed in the mixed layer during the JASIN (1978) experiment to the local wind stress and to the quasi-geostrophic flow field. *Journal of Physical Oceanography*, *12*(10), 1122–1136. https://doi.org/10.1175/1520-0485(1982)012<1122:tronim>2.0.co;2

Whitt, D. B., & Thomas, L. N. (2013). Near-inertial waves in strongly baroclinic currents. *Journal of Physical Oceanography*, *43*(4), 706–725. https://doi.org/10.1175/jpo-d-12-0132.1

Whitt, D. B., & Thomas, L. N. (2015). Resonant generation and energetics of wind-forced near-inertial motions in a geostrophic flow. *Journal of Physical Oceanography*, *45*(1), 181–208. https://doi.org/10.1175/jpo-d-14-0168.1

Zhai, X., Greatbatch, R. J., & Eden, C. (2007). Spreading of near-inertial energy in a 1/12° model of the North Atlantic Ocean. *Geophysical Research Letters*, *34*(10), L10609. https://doi.org/10.1029/2007gl029895

Zhai, X., Greatbatch, R. J., Eden, C., & Hibiya, T. (2009). On the loss of wind-induced near-inertial energy to turbulent mixing in the upper ocean. *Journal of Physical Oceanography*, *39*(11), 3040–3045. https://doi.org/10.1175/2009jpo4259.1

Zhai, X., Greatbatch, R. J., & Sheng, J. (2004). Advective spreading of storm-induced inertial oscillations in a model of the northwest Atlantic Ocean. *Geophysical Research Letters*, *31*(14), L14315. https://doi.org/10.1029/2004gl020084